Front. Chem. Sci. Eng. 2022, 16(4): 546–559
https://doi.org/10.1007/s11705-021-2069-3

RESEARCH ARTICLE

Micromixing performance of the teethed high shear mixer under semi-batch operation

Xiaoning Li[1], Lin Yang[1], Junheng Guo[1], Wei Li[1], Mingliang Zhou (✉)[2], Jinli Zhang (✉)[1,3]

1 School of Chemical Engineering and Technology, Tianjin University, Tianjin 300350, China
2 Department of Geotechnical Engineering, Tongji University, Shanghai 200092, China
3 School of Chemistry and Chemical Engineering, Shihezi University, Shihezi 832003, China

Abstract Semi-batch operated reaction processes are necessary for some competitive reaction systems to achieve a desirable process selectivity and productivity of fine chemical products. Herein the structural and operating parameters of the teethed high shear mixers were adjusted to study the micromixing performance in the semi-batch operated system, using the Villermaux/Dushman reaction system. The results indicate that the rising of the rotor speed and the number of rotor teeth, the decrease of the width of the shear gap and the radial distance between the feed position and the inner wall of stator can enhance the micromixing level and lead to the decrease of the segregation index. Additionally, computational fluid dynamics calculations were carried out to disclose the evolution of the flow pattern and turbulent energy dissipation rate of the semi-batch operated high shear mixer. Furthermore, the correlation was established with a mean relative error of 8.05% and R^2 of 0.955 to fit the segregation index and the parameters studied in this work, which can provide valuable guidance on the design and optimization of the semi-batch operated high shear mixers in practical applications.

Keywords high shear mixer, semi-batch operation, micromixing performance, Villermaux/Dushman system, segregation index

1 Introduction

Extremely fast micromixing of chemical species is one of essential factors to adjust the selectivity and the product yield in competitive consecutive reaction systems [1,2]. In particular, when the mixing time is close to or longer than the inherent reaction time, the micromixing level plays a pivotal role in the distribution of reaction products [1,3–8]. Numerous devices have been proposed to enhance the micromixing performance, including traditional stirred tanks [9,10], spinning disk reactors [11], static reactors [12], rotating packed beds [2,3,13], microchannels [14–16], impinging streams reactors [17], high shear mixers (HSMs) [11,18,19], etc.

HSMs have exhibited potential promising applications to intensify the industrial chemical reaction processes involving pharmaceuticals, cosmetics, food, chemicals, etc. [20–22] since the unique feature of a narrow spacing (0.1–3 mm) between the stator and rotor, high tip speed of the rotor (10–50 $m \cdot s^{-1}$), high shear rate and turbulent energy dissipation rate ε in the gap [11,21,23–25]. The micromixing level of the inline HSM has been explored in detail, reflecting the significant correlations with the structure of the liquid distributor, the shear head structure and operating parameters. For example, Chu et al. [26] intensified the micromixing performance by constructing a novel rotor-stator reactor (RSR), and reported that the micromixing performance in RSR could be improved via adjusting the operating conditions including the rotor speed N and reagent concentration, as well as the structure of rotor-stator head such as the rotor-stator combinations and the number of rotor and stator. Qin et al. [18] conducted a systematically geometrical improvement of the inline HSM to intensify the micromixing performance, considering the structural parameters of the rotor and stator as well as the liquid distributor, and found that liquid distributor can efficiently improve the micromixing performance of the inline HSM. Li et al. [27] designed a novel pore-array liquid distributor to intensify the micromixing performance of the inline HSM. However, to achieve a desirable process selectivity and productivity, semi-batch operated reaction processes are necessary for

Received March 2, 2021; accepted April 30, 2021

E-mails: zhoum@tongji.edu.cn (Zhou M), zhangjinli@tju.edu.cn (Zhang J)

some competitive reaction systems related to fine chemical products [28,29]. So far, the micromixing performance of the semi-batch operated HSM has not been studied intensively yet.

Taking into account the main factors that influence the mixing performance in the batch-operated stirred tanks, involving the feed position, the structure of the rotating component, and the rotating speed, etc. [8,9,30–33], in this article, the structural and operating parameters of the teethed HSM were adjusted to study the micromixing level in the semi-batch operated system, using the Villermaux/Dushman reaction system. Additionally, computational fluid dynamics calculations were carried out to disclose the evolution of the flow pattern and ε of the semi-batch operated HSM. Furthermore, a correlation between segregation index X_s and the investigated parameters was established, which can be used to guide the design and optimization of the semi-batch operated HSMs in practical applications.

2 Experimental

2.1 Experiment apparatus

Figure 1 shows the schematic diagram of experimental apparatus and specific structure. Figures 1(a–c) illustrate the schematic diagram of the experimental apparatus, with four different feed positions of the acid distributed on the plane at 1/2 height of stator teeth (h, mm). The shear head

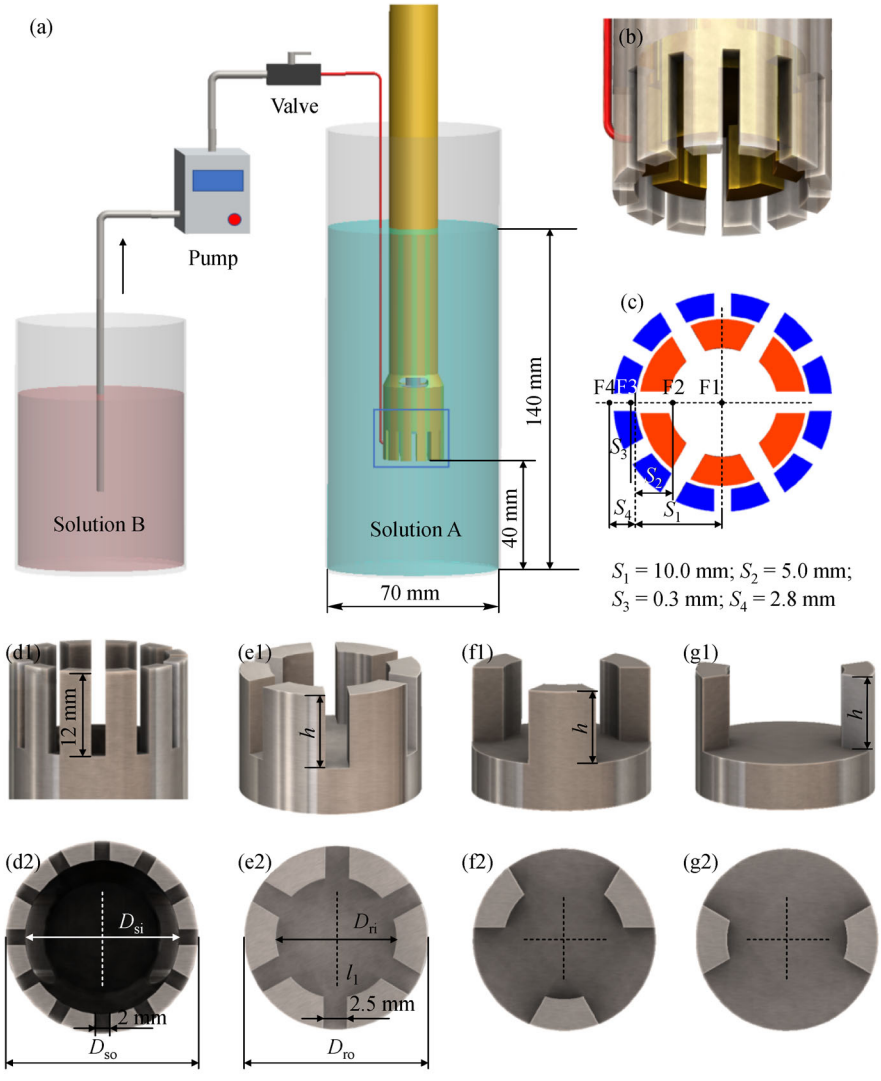

Fig. 1 Schematic diagram of experimental apparatus and specific structure. (a) Schematic diagram of the experimental apparatus; (b) structure diagram of the shear head; (c) section view of shear head; (d) details of the stator head (D_{si} = inner diameter of stator, mm; D_{so} = outer diameter of stator, mm); (e) details of the rotor with 6-teeth (D_{ri} = inner diameter of rotor, mm; D_{ro} = outer diameter of rotor, mm); (f) details of the rotor with 3-teeth; (g) details of the rotor with 2-teeth.

was placed in the center of the tank with an inner diameter D_i of 70 mm, 40 mm above the bottom of the tank. The initial height of the liquid in the tank was 140 mm. And the volume of the liquid in the tank is 500 mL. The teethed HSMs (Fluko-FA30D) were studied, with the detailed structural parameters displayed in Figs. 1(d–g) and Table 1. The teeth sizes are the same in rotors with different numbers of teeth. According to different structural parameters, the HSM is named as "HSM-*n*-*δ*-*h*", where *n* is the number of rotor teeth, *δ* is the width of the shear gap (mm), which refers to the distance between the outer wall of the rotor and the inner wall of the stator. Dilute sulfuric acid solution (solution B) is fed into the mixer through a plunger pump (MP2002C, Shanghai Sanotac Scientific Instruments Co., Ltd.). The outer diameter D_o and D_i of the feed pipe are 1.0 and 0.5 mm, respectively.

Table 1 Main structural parameters of the teethed HSMs

Parameter	Rotor	Stator	Tank
D_i/mm	Φ12.5	Φ20	Φ70
D_o/mm	Φ18, Φ18.5, Φ19	Φ25	Φ75
Teeth gap/mm	2.5	2.0	–
Teeth number	2, 3, 6	12	–
Teeth height/mm	8, 11, 14	12	–

2.2 Experimental materials and procedures

Villermaux/Dushman reaction system [34] was adopted to characterize the mixing performance in the semi-batch operated HSMs. Villermaux/Dushman reaction system includes the following parallel competitive reactions (I–III).

$$H_2BO_3^- + H^+ \rightarrow H_3BO_3 \text{ (instantaneous)} \quad \text{(I)}$$

$$5I^- + IO_3^- + 6H^+ \rightarrow 3I_2 + 3H_2O \text{ (very fast)} \quad \text{(II)}$$

$$I^- + I_2 \rightarrow I_3^- \text{ (quasi-instantaneous)} \quad \text{(III)}$$

During the experiment, the feeding amount of H_2SO_4 solution is controlled to be less than that required to completely react with $H_2BO_3^-$ in the solution A. Under completely mixing conditions, the feed H_2SO_4 solution can be evenly dispersed and reacts with $H_2BO_3^-$ in the solution without participating in the reaction (II). With incomplete mixing conditions, the feed H_2SO_4 solution cannot be evenly dispersed, and the local amount of H^+ cannot be consumed thoroughly by the reaction (I), so that H^+ will partially participate in the reaction (II) to form I_2, and then generate I_3^- through reaction (III).

Table 2 lists the initial concentration of each compound in the solution A and B. The reagents with the analytic purity were used in the experiments. The laboratory temperature was maintained at 17 °C ± 1 °C. Each experiment was repeated at least three times to ensure the accuracy. N varied from 3000 to 12000 r·min^{-1}, and the corresponding rotor tip speed ranged from 2.98 to 11.94 m·s^{-1}. The solution A was laid first in the tank. After the experiment started, 6 mL of the acid solution with H^+ concentration of 1.0 mol·L^{-1} was fed into the tank in most experiments. Only when investigating the influence of H^+ concentration on X_s, the operating conditions of $[H^+]$ = 0.5 mol·L^{-1}, V_B (volume of solution B) = 12 mL and $[H^+]$ = 2 mol·L^{-1}, V_B = 3 mL were adopted. After 2 min, 10 mL mixed solutions were sampled to measure immediately the absorbance at the wavelength of 353 nm by a visible spectrophotometer (723, Shanghai Jinghua Technology Instrument Co., Ltd.).

Table 2 Compositions of the working fluid

Solution	Compound	Concentration/(mol·L^{-1})
Solution A	H_3BO_3	0.1818
	NaOH	0.0909
	KI	0.0117
	KIO_3	0.0023
Solution B	H_2SO_4	0.25, 0.5, 1.0

The concentration of I_3^- in the mixed solution can be calculated through Eq. (1) [34].

$$[I_3^-] = \frac{D_\lambda}{\varepsilon_\lambda l}, \quad (1)$$

where D_λ refers to the absorbance measured at 353 nm. l is the optical path length (10 mm). ε_λ is the molar extinction coefficient, equal to 2620 m^2·mol^{-1} in this work.

The micromixing performance of the reactor can be assessed by the X_s, which is defined as:

$$X_S = Y/Y_{ST}, \quad (2)$$

$$Y = \frac{2(n_{I_2} + n_{I_3^-})}{n_{H_0^+}} = \frac{2V_A([I_2] + [I_3^-])}{V_B[H^+]_0}, \quad (3)$$

$$Y_{ST} = \frac{6[IO_3^-]_0}{6[IO_3^-]_0 + [H_2BO_3^-]_0}, \quad (4)$$

$$X_S = \frac{2(n_{I_2} + n_{I_3^-})/n_{H_0^+}}{6[IO_3^-]_0/(6[IO_3^-]_0 + [H_2BO_3^-]_0)}, \quad (5)$$

where Y represents the ratio of H^+ consumed by reaction (II) to the total H^+, and Y_{ST} represents the theoretical value of Y in complete segregation conditions. n_{I_2} represents molar amount of I_2 in the mixed solution (mol); $n_{I_3^-}$ represents molar amount of I_3^- in the mixed solution (mol); $n_{H_0^+}$ represents molar amount of H^+ fed to the solution A (mol); V_A represents volume of solution A

(mL). Subscript 0 indicates the initial state of the material. X_s varies from 0 to 1. The lower the value of X_s, the better mixing performance.

In addition, the corresponding rate (r_1–r_3) of above three reactions can be expressed in turn by Eqs. (6–8) [7,35].

$$r_1 = k_1[H^+][H_2BO_3^-]$$

$$k_1 = 10^{11}\ m^3\cdot kmol^{-1}\cdot s^{-1}, \quad (6)$$

$$r_2 = k_2[H^+]^2[IO_3^-][I^-]^2, \quad (7)$$

$$r_3 = k_{3+}[I^-][I_2] - k_{3-}[I_3^-], \quad (8)$$

where k_1 is the rate constant of reaction (I) ($L\cdot mol^{-1}\cdot s^{-1}$); k_2 is the rate constant of reaction (II) ($L^4\cdot mol^{-4}\cdot s^{-1}$); k_{3+} is the positive rate constant of reaction (III) ($L\cdot mol^{-1}\cdot s^{-1}$); k_{3-} is the reverse rate constant of reaction (III) (s^{-1}). k_2 is related to the ionic strength (I) of ions in the solution [7,35] from Eq. (9).

$$\log k_2 = \begin{cases} 9.28 - 3.66\sqrt{I} & I < 0.16\ mol\cdot L^{-1} \\ 8.38 - 1.51\sqrt{I} + 0.23I & I > 0.16\ mol\cdot L^{-1} \end{cases}, \quad (9)$$

Recently, Manzano Martínez et al. [36] suggested that when I is less than 0.2 $mol\cdot L^{-1}$ the measurements using the sulfuric acid solution can provide enough accurate results about the micromixing performance. In this work, all the measurements were carried out to meet the condition that I is less than 0.2 $mol\cdot L^{-1}$.

The material balance of the iodine atom is achieved by Eq. (10):

$$[I^-] = [I^-]_0 - \frac{5}{3}([I_2] + [I_3^-]) - [I_3^-]. \quad (10)$$

K_3 can be expressed by Eq. (11):

$$K_3 = \frac{[I_3^-]}{[I_2][I^-]}, \quad (11)$$

and K_3 can be calculated by Eq. (12), which is related to the operating temperature T [37].

$$\lg K_3 = \frac{555}{T} + 7.355 - 2.575\lg T. \quad (12)$$

The concentration of I_2 can be obtained by solving Eq. (13), which is achieved by combining Eqs. (10) and (11).

$$-\frac{5}{3}[I_2]^2 + \left([I^-]_0 - \frac{8}{3}[I_3^-]\right)[I_2] - \frac{[I_3^-]}{K_3} = 0. \quad (13)$$

2.3 Computational fluid dynamics simulation

To deeply understand the flow pattern and the mixing performance of the teethed HSM under semi-batch operation, Ansys Fluent was used to get the flow field and the distribution of ε with different structural parameters. The detailed simulation procedure is described as below.

2.3.1 Simulation method

Previous literature [20,38–41] has proved that the k–ε model can be used to predict the flow characteristics of HSM well. The standard k–ε model is computationally economic and is more widely adopted to simulate the flow characteristics of HSMs [20,38,39,41]. The purpose of the computational fluid dynamics simulations in this study is to get the contour of ε of different structural and operating parameters and to provide an explanation for the experimental results. So the standard k–ε model is chosen in our study. The standard k–ε turbulence model, multiple reference frame method and the standard wall function were used to study the flow fields and ε. The SIMPLE algorithm was applied to solve the discretized N–S equation. The equations were solved in the second-order upwind style. Water was used as the working fluid in the simulation process.

2.3.2 Computational mesh

Figure 2 shows the details of the computational domain and the mesh structure. As illustrated in Fig. 2(a), the calculation domain with the total volume of 5.0×10^{-4} m^3 is composed of the rotational domain and the stationary domain, whose colors are violet and green, respectively. The rotational domain is shown in Fig. 2(c), obtained by wrapping the rotating component shown in Fig. 2(b). The surface 1 and surface 2 marked in Fig. 2(f) are 0.25, 0.1 mm away from the corresponding surfaces of the rotating component, respectively. And the other surfaces of the rotational domain are all 1 mm away from the corresponding surfaces of the rotating component. The interface is made up of the surfaces of the rotational domain. The origin of the coordinate axis is at the center of the upper end surface of the rotor shown in Fig. 2(b). The height of the upper bottom of the rotor is 5 mm. The mesh was generated through Ansys Meshing. To obtain high-quality computational meshes, the entire computational domain is divided into six blocks, as shown in Fig. 2(a). Figures 2(d) and 2(e) show the mesh structure on the plane of $y = 0$ m and $z = 0.01$ m, respectively. The axis of the outlet of the feed pipe is on the plane of $z = 0.01$ m. Four kinds of meshes with different numbers were used to verify mesh independence. Finally, mesh (3) of 5.43 million was used in all cases with the corresponding computational mesh size of 0.01–2 mm.

The mesh independence validation process is performed as follows. HSMs are operated at high speed, which generates the high shear rate and ε in the shear gap between

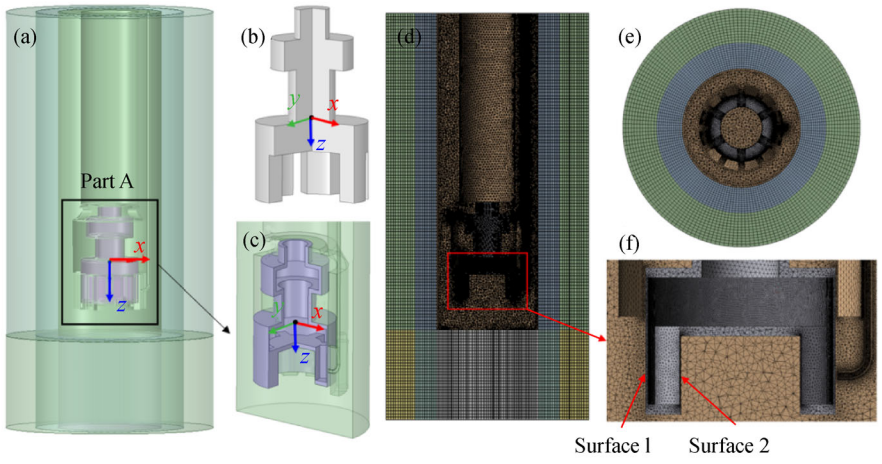

Fig. 2 Details of the calculation domain and mesh structure. (a) Fluid calculation domain of HSM-6-0.5-8; (b) the rotating component; (c) half section view of Part A; (d) the mesh structure of the plane at $y = 0$ m; (e) the mesh structure of the plane at $z = 0.01$ m; (f) enlarged view of the mesh structure of the shear head in the plane of $y = 0$ m.

the stator and rotor. So the ε in the local zone which is close to the gap is worthy of attention. Hence, the local zone close to the gap is marked as Body 1 with a radius of 0.035 m and z-axis coordinates ranging from 0.004 to 0.016 m. The average ε can be calculated by Eq. (14) [19,42]:

$$\overline{\varepsilon}_{\text{Body1}} = \frac{\iiint_V \rho_l \varepsilon \mathrm{d}V}{\rho_l V_{\text{Body1}}}, \tag{14}$$

where ρ_l is the density of the working fluid (kg·m^{-3}), V_{Body1} is the volume of Body 1 (mL), $\overline{\varepsilon}_{\text{Body1}}$ is the average ε of Body 1 (m^2·s^{-3}). Table 3 lists $\overline{\varepsilon}_{\text{Body1}}$. It is obvious that $\overline{\varepsilon}_{\text{Body1}}$ first increases and then reaches a plateau. In addition, the graph shown in Fig. 3 can also be used as criterions for mesh independence verification. Twelve points evenly distributed on a circle in the shear gap with radius of 0.00975 m at z = 0.01 m of HSM-6-0.5-8 are marked in Fig. 3(a), and ε with different mesh numbers are shown in Fig. 3(a). There is little difference in ε between mesh (3) and mesh (4).

Besides, P of the whole computational domain and velocity distribution of z-direction at $y = 0.02$ m are used as auxiliary criteria for mesh independence verification. P can be calculated by Eq. (15) [42].

$$P = \iiint_V \rho_l \varepsilon \mathrm{d}V. \tag{15}$$

The results in Table 3 show that at $N = 6000$ r·min^{-1}, P increases first with the rising number of mesh cells, and then keeps constant after the number of cells exceeds 5.43 million. The velocity distribution of z-direction at $y = 0.02$ m is displayed in Fig. 3(b). It is noted that the velocity distribution of mesh (3) is very similar with mesh (4) but

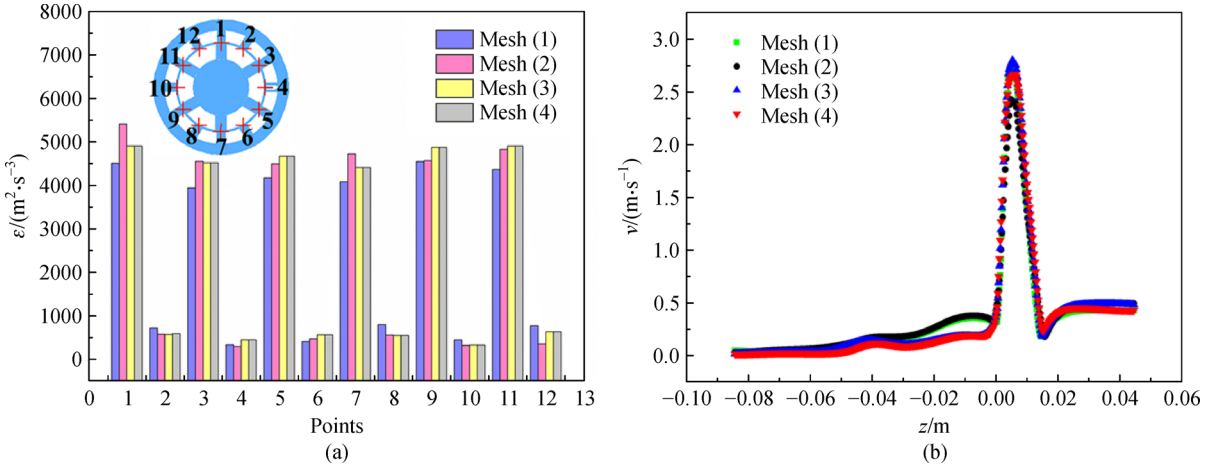

Fig. 3 Diagram for mesh independence verification. (a) ε distribution of 12 points evenly distributed on a circle of the shear gap with a radius of 0.00975 m and $z = 0.01$ m of HSM-6-0.5-8 at $N = 6000$ r·min^{-1}; (b) velocity distribution of $y = 0.02$ m in the z direction of HSM-6-0.5-8 at $N = 6000$ r·min^{-1}.

Table 3 $\bar{\varepsilon}_{Body1}$ from Eq. (14) and power consumption (P) calculated of HSM-6-0.5-8 by Eq. (15) for different mesh structures when N = 6000 r·min^{-1}

Item	Cells	$\bar{\varepsilon}_{Body1}$ /(m^2·s^{-3})	P/W
Mesh (1)	1.51 million	130.99	6.20
Mesh (2)	3.66 million	138.77	6.49
Mesh (3)	5.43 million	144.16	6.88
Mesh (4)	6.51 million	144.41	6.86

different from mesh (1) and mesh (2). In summary, it confirms that mesh (3) used in this work can provide accurate calculations.

3 Results and discussion

3.1 Effect of the injection time of the feed acid on X_s

When the micromixing performance of rotating devices under semi-batch operation is investigated, it must be sure that macromixing and mesomixing are sufficient and materials could not be locally aggregated, which can be achieved by adjusting the injection time of acid [10]. Shorter injection time leads to local accumulation of H^+. In general, X_s of the stirred tanks decreases at first and then keeps constant with the increase of injection time, and the inflection point is called as the critical injection time [7,9,31,33]. The selected injection time of acid solution in the experiments generally exceeds the critical injection time.

Figure 4 shows the effect of the feed rate of acid on X_s and the flow field. The influence of the injection time on X_s under different N can be displayed by Fig. 4(a). At low N ($N \leqslant 4500$ r·min^{-1}), the variation is consistent with the previous description [7,9,31]. However, at high N ($N > 4500$ r·min^{-1}) X_s first decreases, followed by tending to be constant but then increasing with the rising of the injection time. The reason can be explained: when N is high and the flow rate of acid (Q) at the pipe outlet is low, the solution A with strong velocity flows back to the pipe, which leads to the increase of X_s. This phenomenon has also been reported in the literature [43].

To further verify this hypothesis, the flow field simulation was carried out. Figures 4(b–d) can provide an intuitive evidence for the phenomenon of backmixing of the feed pipe. Figure 4(b) shows that the different view of the fluid domain of the teethed HSM and the feed pipe is marked on the section view. Figure 4(c) displays the contours of the velocity vector at the feed pipe of HSM-6-0.5-8 at the feed position F3 under different operating conditions. It indicates that when N = 12000 r·min^{-1} and Q = 1.5 mL·min^{-1}, there is the flow velocity opposite to the main flow direction at the outlet of the feed pipe in Fig. 4(c2), which doesn't appear either in Fig. 4(c1) at the conditions of N = 3000 r·min^{-1} and Q = 1.5 mL·min^{-1} or Fig. 4(c3) at the conditions N = 12000 r·min^{-1} and Q = 12 mL·min^{-1}. To disclose deeply the feed pipe backmixing, the species transport model and the sliding mesh were used in the simulation. There are two fluids in the simulation process, of which physical properties are the same as the water at T = 17 °C. One is presented in the tank to simulate the solution A, and the other is used as the tracer to simulate the acid, fed to the tank by the feed pipe. The contour of mass fraction distribution of the solution A at N = 12000 r·min^{-1} and Q = 1.5 mL·min^{-1} is given in Fig. 4(d). The solution A is dispersed in the feed pipe from Fig. 4(d). It confirms that the solution A would flow back to the feed pipe at high N and low Q. Therefore, each experiment in this work is carried out under the conditions that the influences of macromixing and mesomixing and pipe backmixing are excluded. Table 4 lists Q at different N. In addition, the critical injection time becomes shorter as N increases (Fig. 4(a)). It suggests that the time required for the perfect macromixing decreases with the increase of N. As N increases, the ε increases, and the macromixing proceeds more fully, which is reasonable.

3.2 Effect of acid concentration and N on X_s

Figure 5 shows the effect of the acid concentration and N on X_s and ε. Three acid concentrations ([H^+] = 0.5, 1.0, 2.0 mol·L^{-1}) were chosen to investigate the effect of H^+ concentration on X_s, which is shown in Fig. 5(a). As reported in much literature, X_s increases with the rising of acid concentration [7,9,27]. This is because that the order of H^+ of reaction (II) is higher than that of reaction (I). Hence, by-product increases with rising of H^+ concentration. When [H^+] = 2.0 mol·L^{-1}, the acid volume need to be fed is very small, which might cause larger experimental operation errors. On the contrary, when acid concentration is low, the experimental data changed gently. Therefore, H^+ concentration of 1.0 mol·L^{-1} was chosen in subsequent experiments.

In addition, X_s declines first rapidly and then gently with the increase of N, as shown in Fig. 5(a), which is the same as the previous literature [18,27]. There are contours of ε of HSM-6-0.5-8 under different N (Fig. 5(b)). As N increases, ε increases but X_s declines.

3.3 Effect of the feed position on X_s

It is very important to choose a favorable feed position to enhance the micromixing performance of the semi-batch teethed HSM. It is widely known from previous literature that superior micromixing performance can be obtained in the conditions of high ε [9,44]. Previous studies show that much turbulent energy is dissipated in the shear head of HSM [11,45,46]. Figure 6 displays the effect of feed position on ε and X_s. Computational fluid dynamics

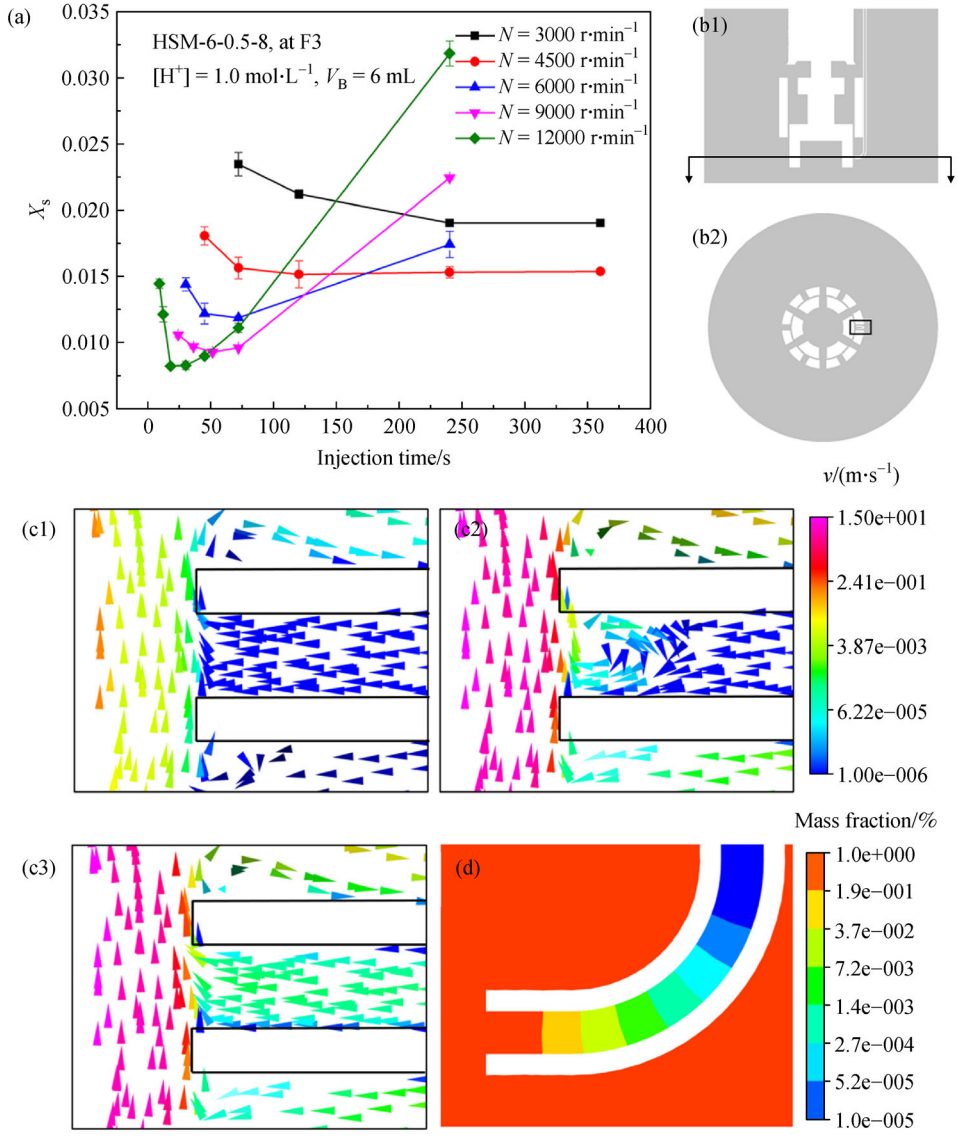

Fig. 4 Effect of injection time of the feed acid on X_s and the flow field. (a) Effect of injection time of the feed acid on X_s; (b1) front view (plane 1) of fluid domain of HSM-6-0.5-8 at the feed position F3; (b2) section view (plane 2) of fluid domain of HSM-6-0.5-8 at the feed position F3; (c) contours of velocity vector at the feed pipe and shear head region of HSM-6-0.5-8 at the feed position F3, under the condition of (c1) when N = 3000 r·min^{-1} and Q = 1.5 mL·min^{-1}; (c2) when N = 12000 r·min^{-1} and Q = 1.5 mL·min^{-1}; (c3) when N = 12000 r·min^{-1} and Q = 12 mL·min^{-1}; (d) Contour of mass fraction distribution of solution A of HSM-6-0.5-8 at feed position F3 when N = 12000 r·min^{-1} and Q = 1.5 mL·min^{-1} when injection time is 0.035 s.

Table 4 Q at different N at F3

N/(r·min^{-1})	Q/(mL·min^{-1})
3000	1.5
4500	1.5
6000	5
9000	8
12000	12

simulation with the sliding mesh of HSM-6-0.5-8 was carried out to get the time-average contour of ε (Fig. 6(a)). It is obvious that high ε appears in the shear head region, which is consistent with the conclusions of previous studies [11,45,46]. According to the contour in Fig. 6(a), four feasible feed positions (aligned with the center of the stator hole) have been chosen, and the distance (S) from the inner wall of the stator is 10 mm (F1), 5.0 mm (F2), 0.3 mm (F3), 2.8 mm (F4), respectively. It is noted that ε

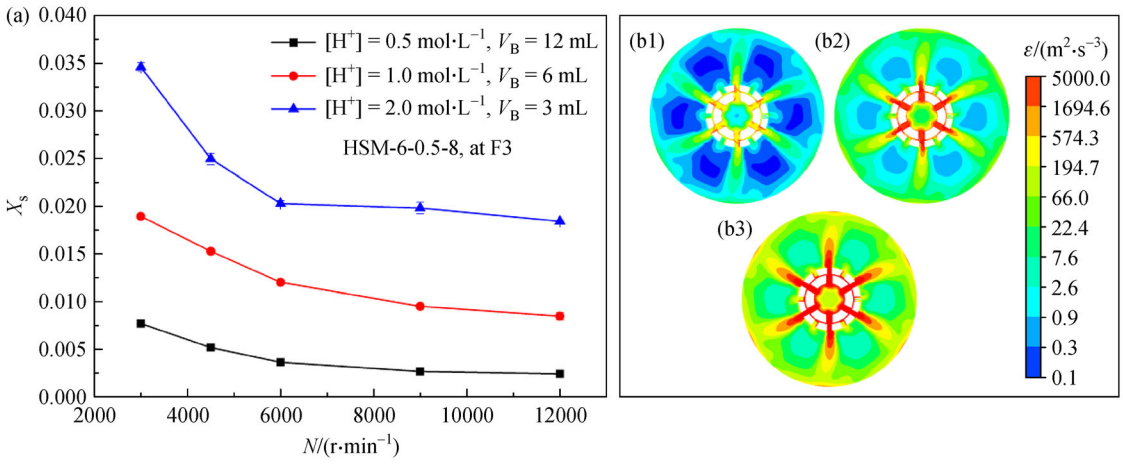

Fig. 5 Effect of acid concentration and N on X_s and ε: (a) Effect of acid concentration and N on X_s; (b) contours of ε of plane 2 of HSM-6-0.5-8 at feed position F3: (b1) N = 3000 r·min^{-1}; (b2) N = 6000 r·min^{-1}; (b3) N = 12000 r·min^{-1}.

becomes stronger with the decrease of S. Figure 6(b) shows that the change of X_s of four feed positions with the rising of N. As we expected, X_s declines with the decrease of S, and the better micromixing performance is obtained at F3.

3.4 Effect of n on X_s

The structure of the rotating component was reported to have an important influence on micromixing [18,31]. The influence of n on the micromixing performance was studied for HSM-n-0.5-8 at the feed position F3. Figure 7 shows the effect of n on X_s and ε. As shown in Fig. 7(a), n is set as 2, 3, and 6, respectively. It indicates that the rising of n contributes to the enhancement of micromixing performance. This is probably due to the increase of n resulting in an increase in the force of rotor teeth on the fluid, which can help to strengthen fluid flow in the rotor and stator holes and shear gap and generate high ε. It can be confirmed in the contours of ε of HSM-n-0.5-8 at feed position F3 and N = 6000 r·min^{-1} (Fig. 7(b)). ε distributed near the shear head and the feed pipe outlet becomes higher with the increase of n, which can intensify micromixing performance.

3.5 Effect of δ on X_s

The shear gap is a vital structural feature of HSM, of which the width determines the strength of the velocity gradient of the fluid in the gap. Figure 8 shows the effect of δ on X_s and ε. The influence of three different δ on the micromixing performance was investigated for HSM-6-δ-8 at the feed position F3 (as shown in Fig. 8(a)), which was adjusted by changing the rotor diameter. Rotors with diameters of 18, 18.5, 19 mm were selected, forming shear gaps of 1.0, 0.75, 0.5 mm with the stator, respectively. It illustrates that X_s decreases with the decrease of δ. Understandably, the fluid can generate a large velocity

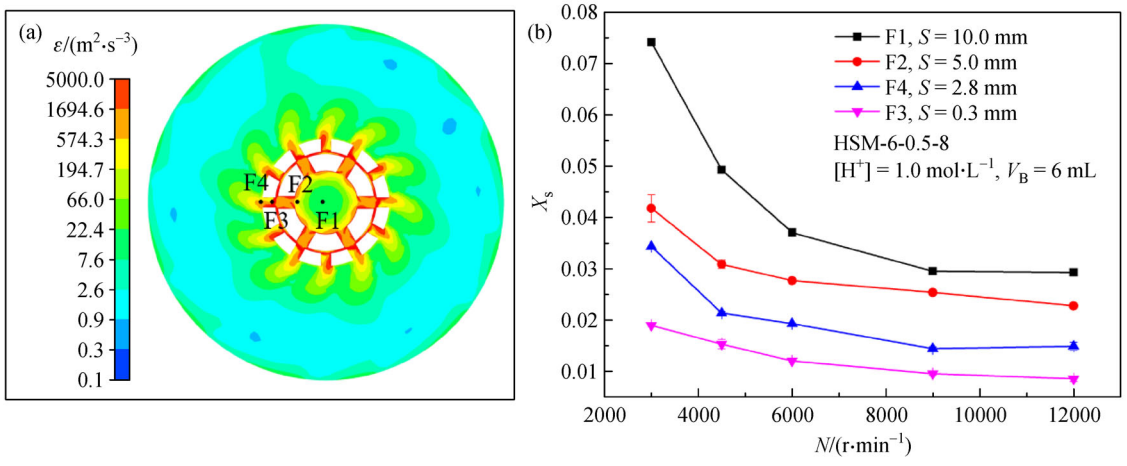

Fig. 6 Effect of feed position on ε and X_s: (a) time-average contours of ε of HSM-6-0.5-8 at N = 6000 r·min^{-1}; (b) effect of feed position on X_s.

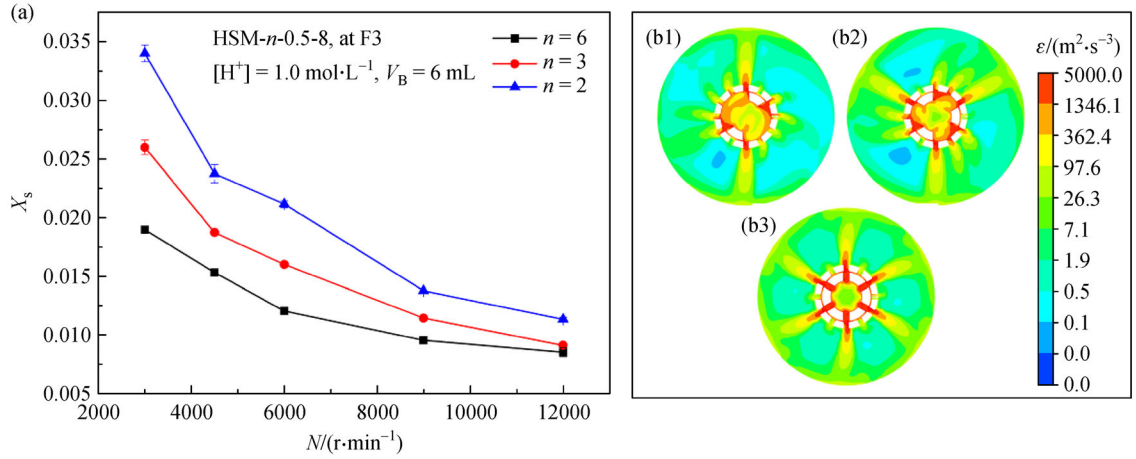

Fig. 7 Effect of n on X_s and ε: (a) effect of n on X_s; (b) contours of ε of plane 2 of HSM-n-0.5-8 at feed position F3 when N = 6000 r·min^{-1}; (b1) n = 2; (b2) n = 3; (b3) n = 6.

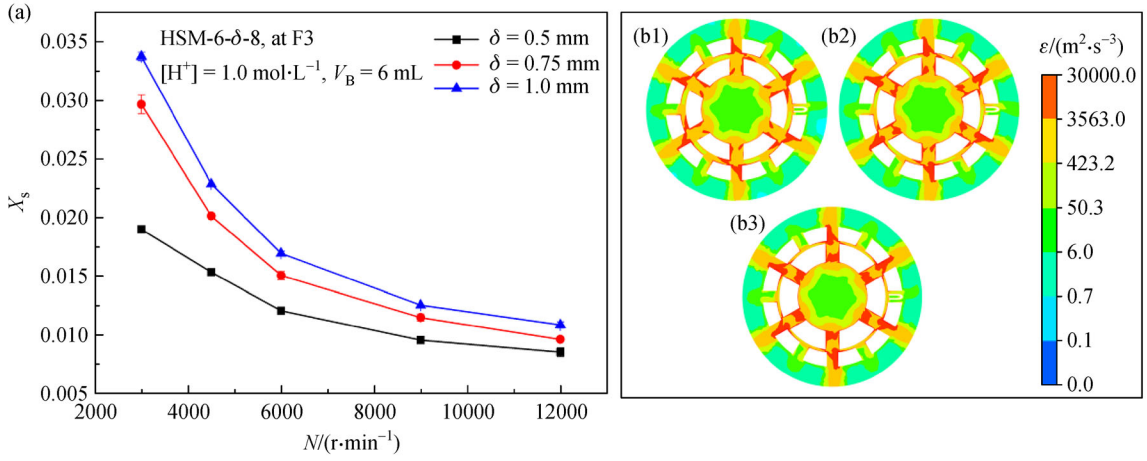

Fig. 8 Effect of δ on X_s and ε: (a) effect of δ on X_s; (b) contours of ε of shear head region of plane 2 of HSM-6-δ-8 at feed position F3 N = 6000 r·min^{-1}; (b1) δ = 1.0 mm; (b2) δ = 0.75 mm; (b3) δ = 0.5 mm.

gradient when flowing in a small shear gap structure, thereby generating high ε, which can intensify micromixing. Figure 8(b) shows contours of ε of HSM-6-δ-8 at feed position F3 and N = 6000 r·min^{-1}. With the decrease of δ, ε at the shear head region increases significantly. The change of ε is consistent with the variation of X_s shown in Fig. 8(a).

3.6 Effect of h on X_s

To understand the influence of h on micromixing performance, three rotors with different teeth heights (h = 8, 11, 14 mm) were chosen. Figure 9 displays the effect of h on X_s and ε. The results (Fig. 9(a)) show that X_s is not much affected by h when $N \geqslant 4500$ r·min^{-1}. Contours of ε of HSM-6-0.5-h at N = 6000 r·min^{-1} are shown in Fig. 9(b). There is little difference in the distribution of ε of HSMs with different h, which confirms that X_s is not affected by h in the semi-batch teethed HSM. This shows that h of the semi-batch teethed HSM is not a critical structural parameter when studying the micromixing performance.

3.7 Correlation to predict X_s

The micromixing performance of HSM is affected by structural and operating parameters as well as fluid physical properties. Specifically, factors influencing the micromixing performance of the semi-batch teethed HSM include N, the structure and size of rotor and stator, the feed position of acid, etc. It is a convenient and concise method to correlate X_s with these parameters, which can provide guidance on improving the micromixing performance. Recently, Liu et al. [33] established a correlation to predict X_s of the coaxial mixers based on Buckingham π theorem, as expressed by Eq. (16).

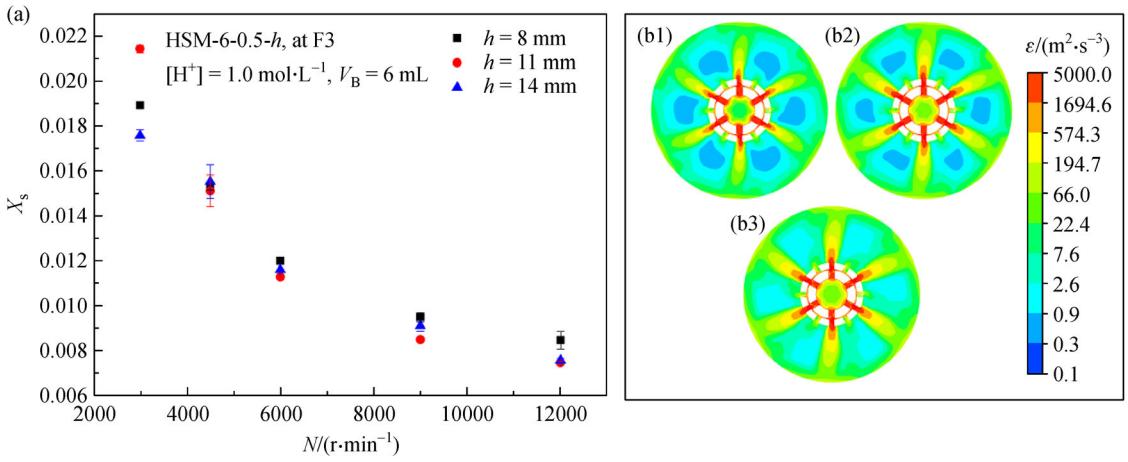

Fig. 9 Effect of h on X_s and ε: (a) effect of h on X_s; (b) contours of the ε of plane 2 of HSM-6-0.5-h when $N = 6000$ r·min^{-1} at feed position F3. (b1) $h = 8$ mm; (b2) $h = 11$ mm; (b3) $h = 14$ mm.

$$X_S = 0.154Sh^{-1.209}Re^{-0.0475}Sc^{1.04}\left(\frac{l}{T}\right)^{0.576}\left(\frac{D}{T}\right)^{0.92}\left(\frac{C}{T}\right)^{0.446}. \quad (16)$$

Since the micromixing level studied by Liu et al. [33] and by us is in the same system and same operation mode, the terms of Sh (Sherwood number), Re (Reynolds number) and Sc (Schmidt number) in Eq. (16) are referred and retained in our correlation. As disclosed by the above experiments, the rising of N and n, the decrease of δ and S can enhance micromixing and lead to the decrease of X_s. Herein the correlation is established as Eq. (17).

$$X_S = c_0 Sh^a Re^b Sc^c \left(\frac{n}{6}\right)^d \left[\left(\frac{S}{D_{si}}\right)^e + f\right]\left(\frac{h}{D_{si}}\right)^g, \quad (17)$$

where c_0 and f are the empirical constants, and a, b, c, d, e, g are the empirical exponents, which are determined by the regression analysis using experimental data (a is exponent of Sh, b is exponent of Sh, c is exponent of Sh, d is exponent of "n/6", and e is exponent of "S/D_{si}"). D_{si} is D_i of the stator (mm).

Re of the HSM is related to the structure of rotor and stator as well as N. Because the structure of the stator remains the same in our work, Re can be calculated by Eq. (18). [47]

$$Re = \frac{\rho_l N D_{ro}{}^2}{\mu}, \quad (18)$$

where N is the rotor speed (r·s^{-1}), D_{ro} is D_o of the rotor (mm), μ is the viscosity of the fluid (Pa·s).

There exist mass transfer processes when the solution B meets with the solution A at the feed position. Acid flows into solution A in the form of tiny spheres. Sh can be achieved by Eq. (19) according to the empirical Eq. [33]:

$$Sh = 0.347Re^{0.62}Sc^{1/3}, \quad (19)$$

where Sc is related to the fluid physical parameters. In this work, fluid physical parameters were not investigated, so the value of exponent c of Sc is inherited from the value of Eq. (16) from the literature [33]. And Sc can be calculated by Eq. (20).

$$Sc = \frac{\mu}{\rho_l D_j}, \quad (20)$$

where D_j is the diffusion coefficient of acid (m^2·s^{-1}).

Since the highest n studied in our study is 6, n is normalized to n/6, which is used to express the influence of n on X_s. Due to the structural parameters of the stator in our study remain unchanged, so S is used to describe the change of feed position, and S is dimensionless to S/D_{si}. It is known that X_s decreases with the decrease of S. But when $S = 0$ mm, X_s is impossible to be 0. To reduce the error of the correlation, a constant term f is added in this term. Hence, "$S/D_{si} + f$" is applied to express the influence of the feed position on X_s. Similarly, h is dimensionless to h/D_{si}, which is employed to express the influence of h on X_s.

Fifty sets of experimental data were used with data regression analysis to calculate the dimensionless number and the corresponding value of X_s based on the differential evolution method and to further determine the coefficients and exponents in the formula. The obtained correlation is expressed by Eq. (21).

$$X_S = 0.416Sh^{-1.113}Re^{-0.0726}Sc^{1.04}\left(\frac{n}{6}\right)^{-0.312}\left[\left(\frac{S}{D_{si}}\right)^{0.919} + 0.224\right]\left(\frac{h}{D_{si}}\right)^{-0.306}. \quad (21)$$

The mean relative error, obtained by averaging the absolute value of the relative error between the 50 sets of

fitted data and the experimental data, equal to 8.05%. R^2 of this correlation is 0.955. The deviation may be due to the empirical calculation formula of *Sh* and *c* adopted in this work to some extent.

From the above research, the rising of n and the decrease of δ can intensify micromixing, so a better micromixing performance is obtained at HSM-6-0.5-8. Table 5 lists X_s of different semi-batch mixers with their best structure, where the concentration of solution A is the same with this work. Figure 10 shows a plot of X_s vs P_v (P per unit volume, W·m^{-3}) of these semi-batch devices. P_v obtained from the simulation results by Fluent. It can be seen from Fig. 10(a) that HSM-6-0.5-8 has a better micromixing performance at the same P_v. On the whole, the semi-batch teethed HSM possesses a lower X_s and a higher P_v.

3.8 Estimation of micromixing time (t_m)

The t_m can evaluate the micromixing performance of reactors, which can be estimated by many mechanism models. Thereinto, the incorporation model [34,48] is widely adopted in many reactors, such as semi-batch stirred tanks [7], inline HSM [18], rotating packed bed [3], etc. It is also adopted in this work, as expressed by Eq. (22).

$$\frac{dC_j}{dt} = (C_{j10} - C_j)\frac{1}{g}\frac{dg}{dt} + R_j, \tag{22}$$

where C_{j10} is the concentration of the substances j in the surrounding fluid (mol·L^{-1}), C_j refers to the concentration of the substances j of the aggregate (mol·L^{-1}), R_j is the generating rate of the substances j of the aggregate (mol·L^{-1}·s^{-1}). The growth rate of the aggregate (g(t)) can be denoted as the exponential form shown in Eq. (23) [18,27].

$$g(t) = \exp(t/t_m), \tag{23}$$

Runge-Kutta method is employed to solve these equations. Assuming that the feed solution is injected to the mixer at once and dispersed evenly, it will cause calculating deviation. Therefore, t_m calculated can only be used to refer to its magnitude for qualitative analysis. The

Table 5 Comparisons of X_s with different mixers

Reactor	Operating conditions	Viscosity/(Pa·s)	Tip velocity/(m·s^{-1})	X_s
Stirred reactor [7]	V_A = 1.0 L, V_B = 4 mL, [H$^+$] = 1 mol·L^{-1}	1.01 × 10^{-3}	0.34–1.72	0.1466–0.2695
Stirred tank using RT [9]	V_A = 24.9 L, V_B = 40 mL, [H$^+$] = 1 mol·L^{-1}	1.01 × 10^{-3}	1.52–2.79	0.0514–0.0720
Stirred tank using MRT [44]	V_A = 24.9 L, V_B = 100 mL, [H$^+$] = 1 mol·L^{-1}	1.01 × 10^{-3}	1.51–2.77	0.0303–0.0552
Torus reactor [10]	V_A = 2.1 L, V_B = 4.2 mL, [H$^+$] = 2 mol·L^{-1}	1.01 × 10^{-3}	0.46–2.73	0.1706–0.5038
Stirred tank with LDB [30]	V_A ≈ 47.4 L, V_B = 32 mL, [H$^+$] = 2 mol·L^{-1}	0.80	0.28–1.40	0.0710–0.3350
HSM-6-0.5-8 (this study)	V_A = 0.5 L, V_B = 6 mL, [H$^+$] = 1 mol·L^{-1}	1.01 × 10^{-3}	2.98–11.94	0.0085–0.0189
	V_A = 0.5 L, V_B = 3 mL, [H$^+$] = 2 mol·L^{-1}	1.01 × 10^{-3}	2.98–11.94	0.0184–0.0346

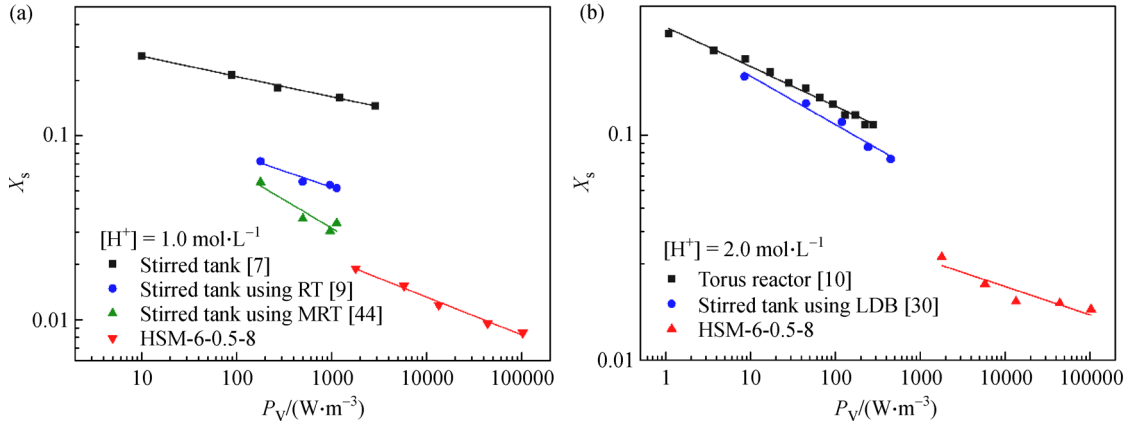

Fig. 10 A plot of X_s vs P_v: comparisons of X_s with various semi-batch devices. (a) [H$^+$] = 1.0 mol·L^{-1}; (b) [H$^+$] = 2.0 mol·L^{-1}.

Table 6 Comparisons of t_m with other HSMs

Ref.	Operation mode	Chemical probe	t_m/s
[49]	Inline	Precipitation of boehmite and NH_4-dawsonite	10^{-3}
[18]	Inline	Villermaux/Dushman reaction	10^{-5}
[27]	Inline	Villermaux/Dushman reaction	10^{-4}
[41]	Inline	Diazo-coupling test reactions	10^{-4}
This work	Semi-batch	Villermaux/Dushman reaction	10^{-4}

relationship between t_m and X_s is $t_m = 0.0619X_s$ with $R^2 = 0.999$ by this calculation method. The variation of X_s ranges from 0.00749 to 0.07416 under $V_B = 6$ mL, $[H^+] = 1.0$ mol·L^{-1} and different structures, and t_m of the semi-batch teethed HSM in this condition is estimated to be 4.63×10^{-4}– 4.5×10^{-3} s. Table 6 shows the comparisons of t_m with other HSMs. The micromixing performance of the other HSMs was all studied in the inline operation mode, which was investigated for the first time in the semi-batch operation mode by this work. The achievable t_m magnitude of HSM-6-0.5-8 is not much different from that in the inline mode.

4 Conclusions

The micromixing performance of the teethed HSM under semi-batch operation has been studied using the iodide-iodate system, combining with computational fluid dynamics simulation. The effects of the structural parameters (n, δ, h) and the operating parameters (N, the feed position, H^+ concentration) on the micromixing performance were studied. The main conclusions obtained are:

1) The effects of operating parameters on the micromixing performance of the teethed HSM under semi-batch operation are as follows: the micromixing performance of the teethed HSM is intensified due to the increase of N and the shorter radial distance between the feed position and the shear gap. X_s decreases as H^+ concentration decreases.

2) The structural parameters of shear head have a significant effect on the micromixing performance of the semi-batch teethed HSM: the micromixing performance is enhanced with the rising of n as well as the decrease of δ. But h doesn't have much impact on X_s. HSM-6-0.5-8 with the feed position F3 has the best micromixing performance.

3) The correlation was established with the mean relative error of 8.05% and R^2 of 0.955 to fit X_s and the parameters studied in our work. This is an effective method to predict the complex law of the micromixing performance in the teethed HSM under semi-batch operation, which is useful to guide the design and optimization of HSMs to improve the micromixing performance in practical applications.

4) t_m of the semi-batch teethed HSMs is estimated to reach 10^{-4} s with the incorporation model, which indicates that the semi-batch teethed HSM has a good micromixing performance with convenience and flexibility.

Acknowledgements This work was financially supported by the National Natural Science Foundation of China (Grant Nos. 22090034, U20A20151, 21776179) and Chemistry and Chemical Engineering Guangdong Laboratory (Grant No. 1922015).

References

1. Bourne J R. Mixing and the selectivity of chemical reactions. Organic Process Research & Development, 2003, 7(4): 471–508
2. Wenzel D, Górak A. Review and analysis of micromixing in rotating packed beds. Chemical Engineering Journal, 2018, 345: 492–506
3. Yang Y C, Xiang Y, Pan C, Zou H K, Chu G W, Arowo M, Chen J F. Influence of viscosity on micromixing efficiency in a rotating packed bed with premixed liquid distributor. Journal of Chemical Engineering of Japan, 2015, 48(1): 72–79
4. Nie A, Gao Z, Xue L, Cai Z, Evans G M, Eaglesham A. Micromixing performance and the modeling of a confined impinging jet reactor/high speed disperser. Chemical Engineering Science, 2018, 184: 14–24
5. Zhang J S, Wang K, Lu Y C, Luo G S. Characterization and modeling of micromixing performance in micropore dispersion reactors. Chemical Engineering and Processing, 2010, 49(7): 740–747
6. Bałdyga J, Pohorecki R. Turbulent micromixing in chemical reactors—a review. Chemical Engineering Journal, 1995, 58(2): 183–195
7. Guichardon P, Falk L. Characterisation of micromixing efficiency by the iodide-iodate reaction system. Part I: experimental procedure. Chemical Engineering Science, 2000, 55(19): 4233–4243
8. Duan X, Feng X, Yang C, Mao Z. CFD modeling of turbulent reacting flow in a semi-batch stirred-tank reactor. Chinese Journal of Chemical Engineering, 2018, 26(4): 675–683
9. Assirelli M, Bujalski W, Eaglesham A, Nienow A W. Study of micromixing in a stirred tank using a rushton turbine. Chemical Engineering Research & Design, 2002, 80(8): 855–863
10. Nouri L, Legrand J, Benmalek N, Imerzoukene F, Yeddou A R, Halet F. Characterisation and comparison of the micromixing efficiency in torus and batch stirred reactors. Chemical Engineering Journal, 2008, 142(1): 78–86
11. Zhang J L, Xu S Q, Li W. High shear mixers: a review of typical applications and studies on power draw, flow pattern, energy

dissipation and transfer properties. Chemical Engineering and Processing, 2012, 57–58: 25–41
12. Fang J Z, Lee D J. Micromixing efficiency in static mixer. Chemical Engineering Science, 2001, 56(12): 3797–3802
13. Yang K, Chu G W, Shao L, Luo Y, Chen J F. Micromixing efficiency of rotating packed bed with premixed liquid distributor. Chemical Engineering Journal, 2009, 153(1–3): 222–226
14. Li W, Xia F, Qin H, Zhang M, Li W, Zhang J. Numerical and experimental investigations of micromixing performance and efficiency in a pore-array intensified tube-in-tube microchannel reactor. Chemical Engineering Journal, 2019, 370: 1350–1365
15. Su Y H, Chen G W, Yuan Q. Ideal micromixing performance in packed microchannels. Chemical Engineering Science, 2011, 66(13): 2912–2919
16. Zha L, Pu X, Shang M J, Li G X, Xu W H, Lu Q H, Su Y H. A study on the micromixing performance in microreactors for polymer solutions. AIChE Journal. American Institute of Chemical Engineers, 2018, 64(9): 3479–3490
17. Hu H, Chen Z, Jiao Z. Characterization of micro-mixing in a novel impinging streams reactor. Frontiers of Chemical Engineering in China, 2009, 3(1): 58–64
18. Qin H Y, Zhang C, Xu Q, Dang X H, Li W, Lei K L, Zhou L T, Zhang J L. Geometrical improvement of inline high shear mixers to intensify micromixing performance. Chemical Engineering Journal, 2017, 319: 307–320
19. Qin H, Xu Q, Li W, Dang X, Han Y, Lei K, Zhou L, Zhang J. Effect of stator geometry on the emulsification and extraction in the inline single-row blade-screen high shear mixer. Industrial & Engineering Chemistry Research, 2017, 56(33): 9376–9388
20. John T P, Panesar J S, Kowalski A, Rodgers T L, Fonte C P. Linking power and flow in rotor-stator mixers. Chemical Engineering Science, 2019, 207: 504–515
21. James J, Cooke M, Kowalski A, Rodgeys T L. Scale-up of batch rotor-stator mixers. Part 2—mixing and emulsification. Chemical Engineering Research & Design, 2017, 124: 321–329
22. James J, Cooke M, Trinh L, Hou R, Martin P, Kowalski A, Rodgers T L. Scale-up of batch rotor-stator mixers. Part 1—power constants. Chemical Engineering Research & Design, 2017, 124: 313–320
23. Vikash V, Deshawar D, Kumar V. Hydrodynamics and mixing characterization in a novel high shear mixer. Chemical Engineering and Processing, 2017, 120: 57–67
24. Yang L, Li W, Guo J, Li W, Wang B, Zhang M, Zhang J. Effects of rotor and stator geometry on dissolution process and power consumption in jet-flow high shear mixers. Frontiers of Chemical Science and Engineering, 2020, 15(2): 384–398
25. Vikash V, Nigam K D P, Kumar V. Design and development of high shear mixers: fundamentals, applications and recent progress. Chemical Engineering Science, 2021, 232: 116296
26. Chu G W, Song Y H, Yang H J, Chen J M, Chen H, Chen J F. Micromixing efficiency of a novel rotor-stator reactor. Chemical Engineering Journal, 2007, 128(2–3): 191–196
27. Li W, Xia F, Zhao S, Guo J, Zhang M, Li W, Zhang J. Mixing performance of an inline high-shear mixer with a novel pore-array liquid distributor. Industrial & Engineering Chemistry Research, 2019, 58(44): 20213–20225
28. Hernandez-Guzman A, Navarro-Gutierrez I M, Melendez-Hernandez P A, Hernandez-Beltran J U, Hernandez-Escoto H. Enhancement of alkaline-oxidative delignification of wheat straw by semi-batch operation in a stirred tank reactor. Bioresource Technology, 2020, 312: 123589
29. Zhang T, Nagy B, Szilágyi B, Gong J, Nagy Z K. Simulation and experimental investigation of a novel supersaturation feedback control strategy for cooling crystallization in semi-batch implementation. Chemical Engineering Science, 2020, 225: 115807
30. Liu B, Zheng Y, Huang B, Qian L, Jin Z. The influence of feeding location on the micromixing performance of novel large-double-blade impeller. Journal of the Taiwan Institute of Chemical Engineers, 2015, 52: 65–71
31. Yang J, Zhang Q, Mao Z S, Yang C. Enhanced micromixing of non-newtonian fluids by a novel zigzag punched impeller. Industrial & Engineering Chemistry Research, 2019, 58(16): 6822–6829
32. Yoshida M, Shimada N, Kanno R, Matsuura S, Otake Y. Liquid flow and mixing in bottom regions of baffled and unbaffled vessels agitated by turbine-type impeller. International Journal of Chemical Reactor Engineering, 2014, 12(1): 629–638
33. Liu B, Sun N, Jin Z, Zhang Y, Sunden B. Numerical investigation and estimating correlation of micromixing performance of coaxial mixers. Industrial & Engineering Chemistry Research, 2019, 58(49): 22376–22388
34. Fournier M C, Falk L, Villermaux J. A new parallel competing reaction system for assessing micromixing efficiency—experimental approach. Chemical Engineering Science, 1996, 51(22): 5053–5064
35. Guichardon P, Falk L, Villermaux J. Characterisation of micromixing efficiency by the iodide-iodate reaction system. Part II: kinetic study. Chemical Engineering Science, 2000, 55(19): 4245–4253
36. Manzano MartÍnez A N, Haase A S, Assirelli M, van der Schaaf J. Alternative kinetic model of the iodide-iodate reaction for its use in micromixing investigations. Industrial & Engineering Chemistry Research, 2020, 59(49): 21359–21370
37. Commenge J M, Falk L. Villermaux-Dushman protocol for experimental characterization of micromixers. Chemical Engineering and Processing, 2011, 50(10): 979–990
38. Jasinska M, Baldyga J, Cooke M, Kowalski A J. Specific features of power characteristics of in-line rotor-stator mixers. Chemical Engineering and Processing, 2015, 91: 43–56
39. John T P, Fonte C P, Kowalski A, Rodgers T L. A comparison of power and flow characteristics between batch and in-line rotor-stator mixers. Chemical Engineering Science, 2019, 202: 481–490
40. Ozcan-Taskin G, Kubicki D, Padron G. Power and flow characteristics of three rotor-stator heads. Canadian Journal of Chemical Engineering, 2011, 89(5): 1005–1017
41. Jasinska M, Baldyga J, Cooke M, Kowalski A. Application of test reactions to study micromixing in the rotor-stator mixer (test reactions for rotor-stator mixer). Applied Thermal Engineering, 2013, 57(1–2): 172–179
42. Duan X, Feng X, Mao Z, Yang C. Numerical simulation of reactive mixing process in a stirred reactor with the DQMOM-IEM model. Chemical Engineering Journal, 2019, 360: 1177–1187
43. Assirelli M, Lee S P, Nienow A W. Further studies of micromixing: scale-up, baffling and feed pipe backmixing. Journal of Chemical Engineering of Japan, 2011, 44(11): 901–907

44. Assirelli M, Bujalski W, Eaglesham A, Nienow A W. Intensifying micromixing in a semi-batch reactor using a Rushton turbine. Chemical Engineering Science, 2005, 60(8–9): 2333–2339
45. Utomo A, Baker M, Pacek A W. The effect of stator geometry on the flow pattern and energy dissipation rate in a rotor-stator mixer. Chemical Engineering Research & Design, 2009, 87(4A): 533–542
46. Utomo A T, Baker M, Pacek A W. Flow pattern, periodicity and energy dissipation in a batch rotor-stator mixer. Chemical Engineering Research & Design, 2008, 86(12A): 1397–1409
47. Hall S, Cooke M, El-Hamouz A, Kowalski A J. Droplet break-up by in-line Silverson rotor-stator mixer. Chemical Engineering Science, 2011, 66(10): 2068–2079
48. Villermaux J, Falk L. A generalized mixing model for initial contacting of reactive fluids. Chemical Engineering Science, 1994, 49(24): 5127–5140
49. Lafficher R, Digne M, Salvatori F, Boualleg M, Colson D, Puel F. Influence of micromixing time and shear rate in fast contacting mixers on the precipitation of boehmite and NH_4-dawsonite. Chemical Engineering Science, 2018, 175: 343–353